Journal of Power Sources 182 (2008) 642–652

Contents lists available at ScienceDirect

Journal of Power Sources

journal homepage: www.elsevier.com/locate/jpowsour

Pseudocapacitive properties of electrochemically prepared nickel oxides on 3-dimensional carbon nanotube film substrates

Kyung-Wan Nam [a,b], Kwang-Heon Kim [a], Eun-Sung Lee [a], Won-Sub Yoon [b], Xiao-Qing Yang [b], Kwang-Bum Kim [a,*]

[a] Division of Materials Science and Engineering, Yonsei University, 134 Shinchon-dong, Seodaemoon-gu, Seoul 120-749, Republic of Korea
[b] Chemistry Department, Brookhaven National Laboratory, Upton, NY 11973, USA

ARTICLE INFO

Article history:
Received 8 January 2008
Received in revised form 12 March 2008
Accepted 31 March 2008
Available online 25 April 2008

Keywords:
Electrochemical capacitor
Supercapacitor
Nanocomposite

ABSTRACT

Nickel oxides on carbon nanotube electrodes (NiO_x/CNT electrodes) are prepared by depositing $Ni(OH)_2$ electrochemically onto carbon nanotube (CNT) film substrates with subsequent heating to 300 °C. Compared with the as deposited $Ni(OH)_2$ on CNT film substrates ($Ni(OH)_2$/CNT electrodes), the 300 °C heat treated electrode shows much high rate capability, which makes it suitable as an electrode in supercapacitor applications. X-ray photoelectron spectroscopy shows that the pseudocapacitance of the NiO_x/CNT electrodes in a 1 M KOH solution originates from redox reactions of NiO_x/NiO_xOH and $Ni(OH)_2$/NiOOH. The 8.9 wt.% NiO_x in the NiO_x/CNT electrode shows a NiO_x-normalized specific capacitance of 1701 F g^{-1} with excellent high rate capability due to the 3-dimensional nanoporous network structure with an extremely thin NiO_x layer on the CNT film substrate. On the other hand, the 36.6 wt.% NiO_x/CNT electrode has a maximum geometric and volumetric capacitance of 127 mF cm^{-2} and 254 F cc^{-1}, respectively, with a specific capacitance of 671 F g^{-1}, which is much lower than that of the 8.9% NiO_x electrode. This decrease in specific capacitance of the high wt.% NiO_x/CNT electrodes can be attributed to the dead volume of the oxides, high equivalent series resistance for a heavier deposit, and the ineffective ionic transportation caused by the destruction of the 3-dimensional network structure. Deconvolution analysis of the cyclic voltammograms reveals that the rate capability of the NiO_x/CNT electrodes is adversely affected by the redox reaction of $Ni(OH)_2$, while the adverse effects from the reaction of NiO_x is insignificant.

1. Introduction

Recently, electrochemical capacitors (ECs) have attracted considerable attention for use in high power energy storage devices. Electrochemical capacitors have potential applications including power enhancement and primary or hybrid power sources combined with batteries and fuel cells for the hybrid electric vehicle (HEV) or fuel cell electric vehicle (FCEV). In these ECs, the energy stored is either capacitive or pseudocapacitive in nature. The capacitive or non-Faradaic process is based on charge separation at the electrode/solution interface. On the other hand, the pseudocapacitive process consists of Faradaic redox reactions that occur within the active electrode materials. Carbon, conducting polymers and transition metal oxides are the most widely used active electrode materials [1,2]. Hydrous RuO_2 exhibits the best properties among the many transition metal oxide materials investigated as pseudocapacitor (or supercapacitor) materials thus far. An amorphous phase of $RuO_2 \cdot xH_2O$ formed using a sol–gel method at low temperatures shows a specific capacitance as high as 720 F g^{-1} in an acidic electrolyte [3]. However, its commercial use is limited by its high cost. Therefore, there has been considerable effort on the search for alternative electrode materials, such as cobalt oxide [4], manganese oxide [5–9], and nickel oxide [10–17], which are inexpensive and show similar pseudocapacitive behavior to hydrous RuO_2.

Nickel oxide is considered a potential electrode material for supercapacitors in alkaline electrolytes on account of its easy synthesis and relatively high specific capacitance (mass-normalized capacitance, F g^{-1}). However, nickel oxide has the significant drawback of a small operating potential window (~0.5 V). This can be overcome by adapting an asymmetric EC configuration, which employs nickel oxide as the positive electrode and another material as the negative electrode [18–20]. Nickel oxides as a supercapacitor electrode material can be prepared using a variety of synthetic routes, such as the thermal treatment of an electrodeposited or sol–gel prepared nickel hydroxide [10–14], liquid crystal templating electrodeposition [15], simple liquid-phase process [16], and the replication of a mesoporous silica template [17]. The specific

* Corresponding author. Tel.: +82 2 2123 2839; fax: +82 2 312 5375.
E-mail address: kbkim@yonsei.ac.kr (K.-B. Kim).

0378-7753/$ – see front matter © 2008 Elsevier B.V. All rights reserved.
doi:10.1016/j.jpowsour.2008.03.090

capacitance of nickel oxide electrode materials ranges from 50 to 350 F g^{-1} (from a single electrode) depending on the method of synthesis, which is still far from the theoretical value of 2584 F g^{-1} within 0.5 V.

A literature review of composite electrodes made from transition metal oxides and carbonaceous materials [21–28] showed that metal oxides can be produced with a high specific capacitance and rate capability. This is particularly so when a small amount of metal oxide is dispersed uniformly over a conducting and porous carbonaceous material with a very high surface area due to the increased electrical conductivity, electrochemical utilization of the metal oxide and ionic transport throughout the internal volume of the electrode. Based on this concept, a NiO_x coating on a carbon nanotube (CNT) film substrate with a 3-dimensionally interconnected network structure was previously synthesized [23]. The NiO_x-normalized specific capacitance of the NiO_x coated CNT electrode (i.e., NiO_x/CNT electrode) was reported to be ~1000 F g^{-1}, which is approximately three times higher than the ~350 F g^{-1} obtained for the NiO_x thin film electrode [23]. This high specific capacitance of the NiO_x/CNT electrode was attributed to the construction of an electrode with a nanometer-thick NiO_x layer on a CNT film substrate, which has a 3-dimensional network structure.

In contrast to the viewpoint of the electrochemical utilization of nickel oxides, the oxide loading in the electrode should also be considered for practical applications, particularly for large capacitor applications, such as power sources for the HEV or FECV. Hence, there is a need for an electrode with a higher volumetric capacitance (volume-normalized capacitance, F cm^{-3}) and geometric capacitance (area-normalized capacitance, F cm^{-2}), which are generally proportional to the loading of the active material, with little sacrifice of the specific capacitance. In the case of the NiO_x/CNT nanocomposite electrode, it is believed that the specific, geometric and volumetric capacitances will be affected by the microstructure of the electrode, which is closely related to the oxide loading. Therefore, this study examined the effects of the NiO_x loading on the microstructure and corresponding electrochemical properties of NiO_x/CNT electrodes, i.e. the geometric, volumetric and specific capacitance. In order to provide a clearer understanding of the electrochemical properties of the nanostructured nickel oxide electrode for potential use in supercapacitors, the detailed electrochemical redox reaction of the NiO_x/CNT electrode in a 1 M KOH solution was also examined by X-ray photoelectron spectroscopy (XPS) and deconvolution analysis of the cyclic voltammograms (CVs).

2. Experimental

CNT films with a 3-dimensional nanoporous network structure were deposited onto a Pt coated Si wafer using an electrostatic spray deposition (ESD) technique [23,27–29]. A CNT film coated Pt/Si wafer was used as a substrate for the electrochemical preparation of nickel oxide. The process for preparing the CNT film substrate is described elsewhere [23,27–29]. The multi-walled carbon nanotubes (MWNTs) were supplied from ILJIN Nanotech Co., Ltd. The thickness and mass of the CNT film used as the substrate were ~5.0 μm and ~0.35 mg cm^{-2}, respectively. The nominal area of the CNT film was 1 × 1 cm^2. The CNT film was pre-heated to 300 °C for 1 h to remove surface-adsorbed species, such as H_2O and hydrocarbon.

The nickel oxides on the CNT film substrate were formed by depositing $Ni(OH)_2$ through galvanostatic pulse deposition followed by heat treatment in air at 300 °C for 1 h. A pulsed electrodeposition method was used to obtain uniform $Ni(OH)_2$ coatings on the nanoporous CNT film substrate. After the initial application of −4 mA cm^{-2} for 15 s, a pulse current with an amplitude of −4 mA cm^{-2} was applied for various cycles to control the mass of the deposit. The pulse-on and pulse-off times were 0.3 and 2.1 s, respectively. The optimal heat treatment temperature of the nickel oxide thin film electrode was reported to be 300 °C. A previous X-ray absorption spectroscopy study reported that the nickel oxides heated at 300 °C are non-stoichiometric (NiO_x) [13]. An as-deposited $Ni(OH)_2$ coated on the CNT film substrate ($Ni(OH)_2$/CNT electrode) was also prepared for comparison. The reported weight of the nickel oxide is the difference between the weight of the bare substrate before nickel oxide deposition and that of the nickel oxide deposited substrate after annealing, which was measured to an accuracy of 0.1 μg using a microbalance (Sartorius SC2, Germany).

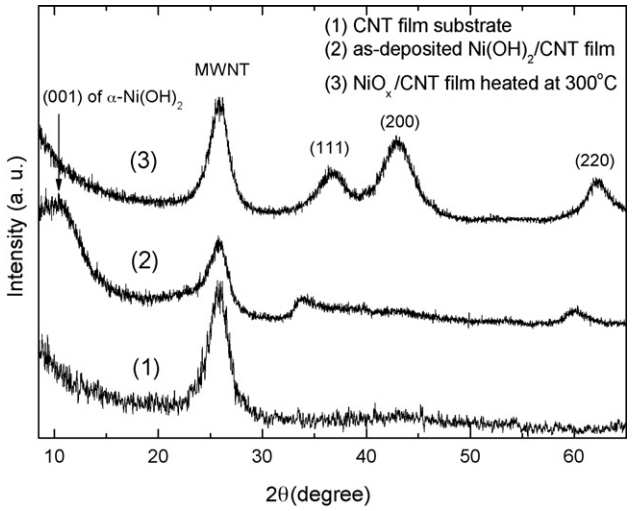

Fig. 1. XRD patterns of the CNT film substrate, as-deposited $Ni(OH)_2$/CNT electrode and NiO_x/CNT electrode heated at 300 °C.

The crystal structure of the nickel oxide/CNT film electrodes was examined by glancing angle X-ray diffraction. The patterns were recorded on a Rigaku DMAX-2500 diffractometer using Cu $K_{\alpha 1}$ radiation with a glancing incident angle of 1°. The surface morphology of the NiO_x coated on the CNT film was examined by field-emission scanning electron microscopy (SEM, SIRION^{TM}, FEI COMPANY). X-ray photoelectron spectroscopy (XPS) was carried out using an ESCALAB 220i-XL (FISONS instruments) system with a Mg K_α source (1253.6 eV). The data was referenced to the 284.6 eV peak for C 1s. The cyclic voltammetry experiments were conducted using a multichannel potentiostat (VMP2, Princeton Applied Research, USA) to determine the electrochemical properties of the NiO_x/CNT electrodes in a 1 M KOH solution. Unless otherwise noted, all cyclic voltammograms were recorded after 10 conditioning cycles in 1 M KOH at 30 mV s^{-1}.

3. Results and discussion

3.1. Comparison of the electrochemical properties of the bare CNT film, $Ni(OH)_2$/CNT, and NiO_x/CNT electrodes

Fig. 1 shows the XRD patterns of the CNT film substrate, as-deposited $Ni(OH)_2$ coated on CNT film (i.e., $Ni(OH)_2$/CNT electrode) and NiO_x coated CNT film (i.e., NiO_x/CNT electrode), which was produced by heating the $Ni(OH)_2$/CNT films to 300 °C for 1 h. The characteristic graphitic (0 0 2) peak of the MWNT at 26° was clearly observed on the CNT film substrate [30]. The XRD pattern of the as–deposited $Ni(OH)_2$/CNT electrode corresponded to the well-known layered α-$Ni(OH)_2$ structure with a characteristic (0 0 1) peak at 10.2° along with a relatively weak MWNT peak at 26°. The characteristic peaks for rock salt NiO at 37°, 43° and 63° as well

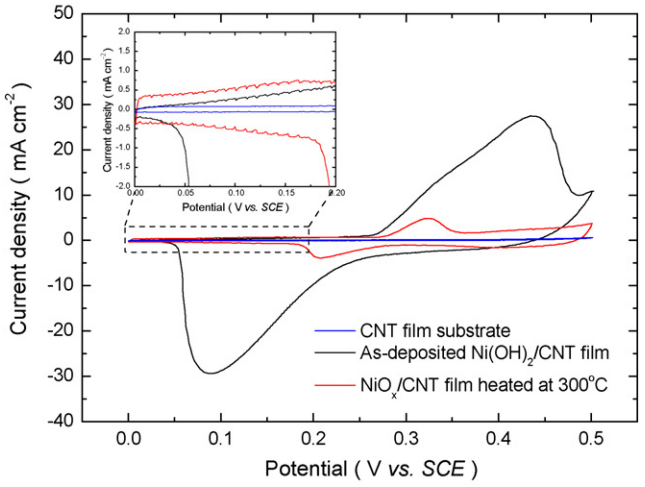

Fig. 2. CVs of the CNT film substrate, as-deposited $Ni(OH)_2$/CNT electrode and NiO_x/CNT electrode. The CVs were measured in 1 M KOH at a scan rate of 10 mV s^{-1}. Inset: enlarged view of the CVs with a potential window of 0.0–0.2 V *vs. SCE*.

as the MWNT at 26° were observed in the XRD patterns of the NiO_x/CNT electrode heated at 300 °C. This confirmed that nickel oxide with a rock salt structure had formed on the CNT film substrate after heating the $Ni(OH)_2$/CNT electrode to 300 °C, which agrees well with that of the NiO_x thin film electrode deposited on a Pt foil substrate [12,13].

The electrochemical properties of the CNT film substrate, $Ni(OH)_2$/CNT and NiO_x/CNT electrodes were compared by performing cyclic voltammetry in a 1 M KOH solution. The weight fraction of $Ni(OH)_2$ and NiO_x on the $Ni(OH)_2$/CNT and NiO_x/CNT electrodes were ~18 and 20%, respectively. The electrode potential was scanned between 0.0 and 0.5 V *vs. SCE* at 10 mV s^{-1}. Fig. 2 shows the CVs of the three electrodes. The CV of the as-deposited $Ni(OH)_2$/CNT electrode showed a set of large redox peaks corresponding to the nickel oxidation/reduction reaction. This can be as the reaction below, which involves the intercalation/deintercalation of protons.

$$Ni(OH)_2 + OH^- \underset{\text{discharge}}{\overset{\text{charge}}{\Leftrightarrow}} NiOOH + H_2O + e^-, \quad (1)$$

When the $Ni(OH)_2$/CNT electrode was heated to 300 °C, the capacity decreased significantly and the current–potential responses were symmetric about the zero-current axis. However, the anodic current responses of the $Ni(OH)_2$/CNT electrode between 0.0 and 0.2 V *vs. SCE* were smaller than those of the heated NiO_x/CNT electrode, which are shown in the inset in Fig. 2. Although the cathodic current–potential responses of the $Ni(OH)_2$/CNT electrode were complicated by the redox reaction (1), the current–potential responses of the NiO_x/CNT electrode between 0.0 and 0.2 V *vs. SCE* appeared to be more reversible than those of the $Ni(OH)_2$/CNT electrode. Similar results were also observed in a previous study on a $Ni(OH)_2$ and NiO_x thin film electrode on a Pt foil substrate [23]. Compared with the $Ni(OH)_2$/CNT and NiO_x/CNT electrodes, the bare CNT film electrode showed a relatively small current response originating from double layer charging/discharging on the CNT surface. The capacitive current of the NiO_x/CNT electrode between 0.0 and 0.2 V *vs. SCE* (shown in the inset of Fig. 2) were much larger than those of the bare CNT electrode, even though the mass of the CNT in both electrodes was similar, ~0.36 mg cm^{-2}. Therefore, the enhanced capacitive current of NiO_x/CNT electrode was attributed to the Faradaic pseudocapacitance of the NiO_x coating on the CNT film substrate.

Due to the existence of a set of redox peaks, the voltammetric current responses of the NiO_x/CNT electrode in Fig. 2 showed different CV features to those of the NiO_x thin film electrodes, which had been deposited on metal foil or low surface area graphite substrates and showed featureless and capacitive current responses in the CVs [23]. The anodic and cathodic redox peaks appear at ~0.33 and 0.19 V *vs. SCE* in the CV, respectively. The origin of these redox peaks was examined by XPS and will be discussed in the next section. Capacitive current responses were observed on the anodic sweep between 0.0 and 0.3 V *vs. SCE* and the cathodic sweep between 0.25 and 0.5 V *vs. SCE*. The capacitive currents of NiO_x were previously attributed to the surface redox reaction of the nickel oxides as follows: [10,11]

$$NiO_x + yOH^- \underset{\text{discharge}}{\overset{\text{charge}}{\Leftrightarrow}} NiO_x(OH)_y + ye^- \quad (2)$$

A good high rate capability is an important property of an electrode used in supercapacitors for high power applications. The rate capability of the $Ni(OH)_2$/CNT and NiO_x/CNT electrodes was examined using cyclic voltammetry in a 1 M KOH solution at various scan rates. Fig. 3(a) and (b) shows the CVs of the $Ni(OH)_2$/CNT and NiO_x/CNT electrodes at scan rates ranging from 10 to 100 mV s^{-1}, respectively. In the case of the $Ni(OH)_2$/CNT electrode, the redox peaks were no longer visible in the CVs, and the shape of the CVs was seriously distorted at scan rates ≥30 mV s^{-1}, indicating resistive behavior. The diffusion process of the protons in the hydroxide layer is the rate determining step of the $Ni(OH)_2$/NiOOH redox reaction. Although there are rich CNT channels in the $Ni(OH)_2$/CNT electrode that are electronically conducting, the rate capability can be problematic if the proton is unable to participate in the redox reaction over the whole hydroxide layer for a given time corresponding to the potential scan rate. Moreover, even though the electrical conductivity of the nickel hydroxide electrode increases with the state of charge, the insulating nature of the $Ni(OH)_2$, which has an extremely low conductivity in the order of 10^{-17} S cm^{-1}, can also adversely effect the rate capability of $Ni(OH)_2$/CNT electrodes [31]. On the other hand, the CVs of the NiO_x/CNT electrode shown in Fig. 3(b) are highly reversible regardless of the potential scan rates. The shape of the CVs of the NiO_x/CNT electrode was maintained with increasing scan rate, even though there was a set of redox reaction peaks showing the high kinetic reversibility of the NiO_x/CNT electrode. More detailed analysis of the capacitive currents of NiO_x as well as the cathodic and anodic redox peaks in the NiO_x/CNT electrode will be discussed in the Section 3.3.

Fig. 3(c) shows a plot of the normalized capacity vs. the scan rate of the $Ni(OH)_2$/CNT and NiO_x/CNT electrodes to give a clear comparison of the rate capability of both electrodes. First, the specific capacitance of the electrodes was determined by calculating the whole cathodic charge in the CVs shown in Fig. 3, and then dividing this charge by the potential window of 0.5 V and the mass of the oxides deposited. The normalized capacitance at each scan rate was obtained by dividing the specific capacitance of the electrodes at each potential scan rate by the specific capacitance measured at 10 mV s^{-1}. There was a 93 and 12% decrease in the normalized capacity of the $Ni(OH)_2$/CNT and NiO_x/CNT electrodes with increasing scan rate from 10 to 100 mV s^{-1}, respectively. This highlights the potential applications of the NiO_x/CNT electrode in high-power supercapacitors.

3.2. XPS study on the origin of redox peaks in the CV of the NiO_x/CNT electrode

It was reported that similar redox peaks observed in the CVs of the NiO_x/CNT electrode are often observed in the CVs of pseudocapacitive nickel oxides, particularly for oxides with a high

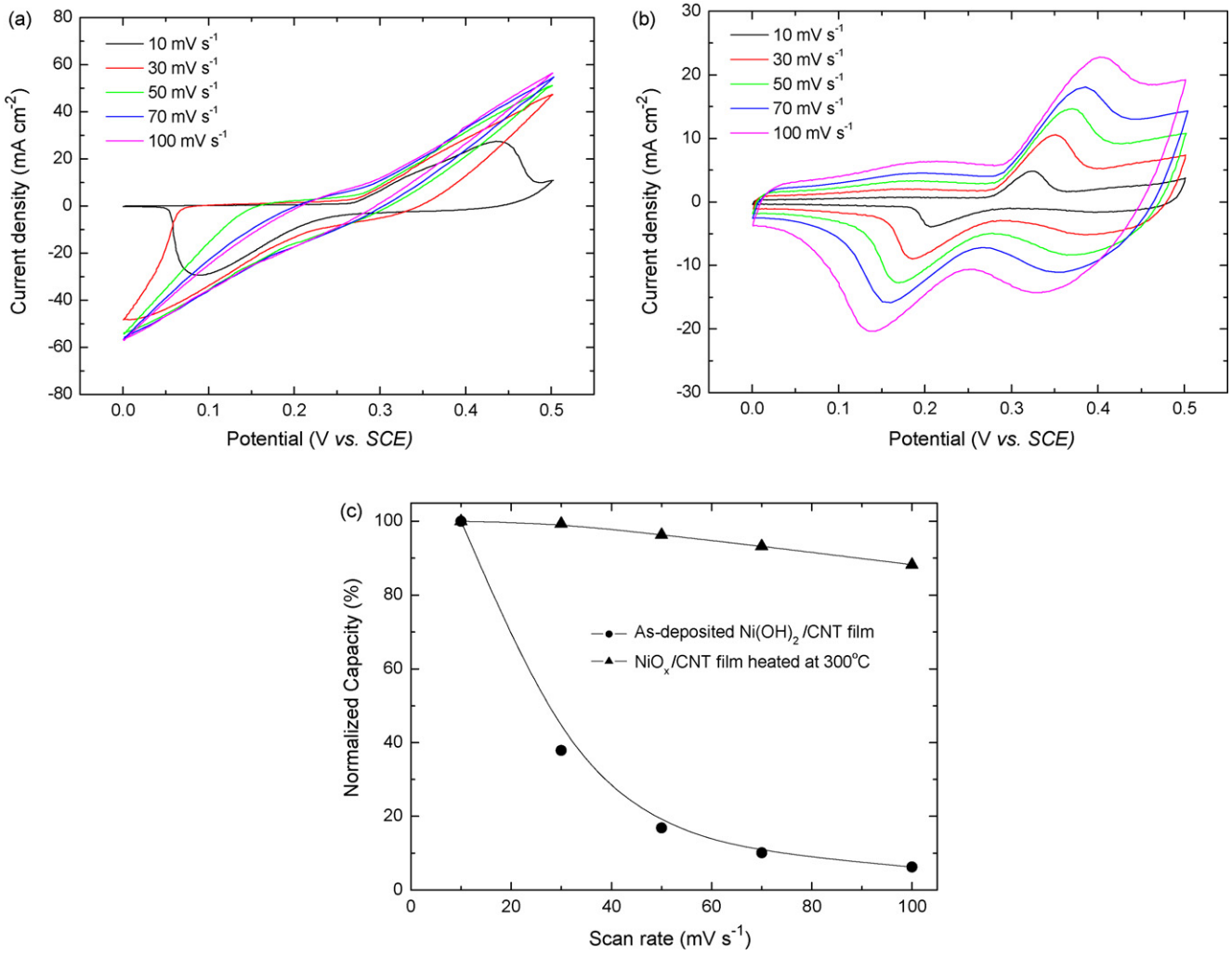

Fig. 3. CVs of (a) as-deposited $Ni(OH)_2$/CNT electrode and (b) NiO_x/CNT electrode at various scan rates between 10 to 100 mV s^{-1}. (c) Comparison of the normalized charges of the as-deposited $Ni(OH)_2$/CNT and NiO_x/CNT electrodes at various scan rates between 10 and 100 mV s^{-1}.

surface/bulk ratio, such as thin film electrodes [11], mesoporous nickel/nickel oxide [15], nanocrystalline NiO [16], and ordered mesoporous NiO [17]. Although a few papers have mentioned these redox peaks, their origin is unclear [11,23]. Therefore, XPS was used to examine the origin of the anodic and cathodic peaks appearing in the CV of the NiO_x/CNT electrode heated to 300 °C. The as-prepared NiO_x/CNT electrode and NiO_x/CNT electrode after 500 CV cycles at 30 mV s^{-1} in 1 M KOH were examined by XPS. The intensity of these redox peaks increased slightly with CV cycling in the potential window of 0.0–0.5 V *vs. SCE*. Therefore, extensive CV cycling (e.g., 500 cycles) was carried out to facilitate the redox reaction, and enhance the sensitivity of the corresponding chemical shift in the XP spectra. Fig. 4(a) shows the CVs of the NiO_x/CNT electrode measured for 500 cycles. Interestingly, the intensity of each redox peak increased with increasing number of cycles, and the capacitive currents remained relatively unchanged. A detailed examination into the mechanism for the increase in the redox peak currents of nickel oxide electrodes during cycling using electrochemical quartz crystal microbalance (EQCM) measurements is currently underway.

Fig. 4(b)–(e) shows the curve-fitted Ni $2p_{3/2}$ and O 1s XP spectra of the as-prepared NiO_x/CNT electrode and cycled NiO_x/CNT electrode. The typical satellite features marked as "S" in Fig. 4(b) and (d) were observed at the ~7 eV high binding energy side of the Ni $2p_{3/2}$ lines, which are associated with octahedral, high spin Ni^{2+} in the NiO_x structure [32]. Table 1 lists the binding energy (Ni $2p_{3/2}$ and O 1s region) and relevant atomic ratios obtained from the NiO_x/CNT electrodes before and after CV cycling from a deconvolution of the XP spectrum. As shown in Fig. 4(b) and Table 1, curve fitting of the Ni $2p_{3/2}$ XP signal for the as-prepared NiO_x/CNT electrode showed different nickel species with binding energies of 853.7, 855.3, and 857.1 eV, which were assigned to NiO (Ni^{2+}), $Ni(OH)_2$ (Ni^{2+}) and Ni_2O_3 (Ni^{3+}), respectively [33]. The relative composition of NiO, $Ni(OH)_2$ and Ni_2O_3 in the as-deposited NiO_x/CNT electrode were 59.9, 35.4 and 4.7%, respectively, which shows NiO to be the main component of the as-deposited NiO_x/CNT electrode. The contribution from $Ni(OH)_2$ observed in the XP spectra of the as-deposited NiO_x/CNT electrode is probably due to the hydration of the nickel oxide surface due to air exposure. In addition, the

Table 1
XPS results of the as-deposited and cycled NiO_x/CNT electrodes

		Ni $2p_{3/2}$			O 1s	
		1	2	3	1	2
As-deposited NiO_x/CNT	Binding energy (eV)	853.7	855.3	857.1	529.1	530.8
	Relative ratio (%)	59.9	35.4	4.7	37.2	62.8
500 cycled NiO_x/CNT	Binding energy (eV)	853.8	855.6		529.4	531.2
	Relative ratio (%)	24.5	75. 5		14.5	85.5

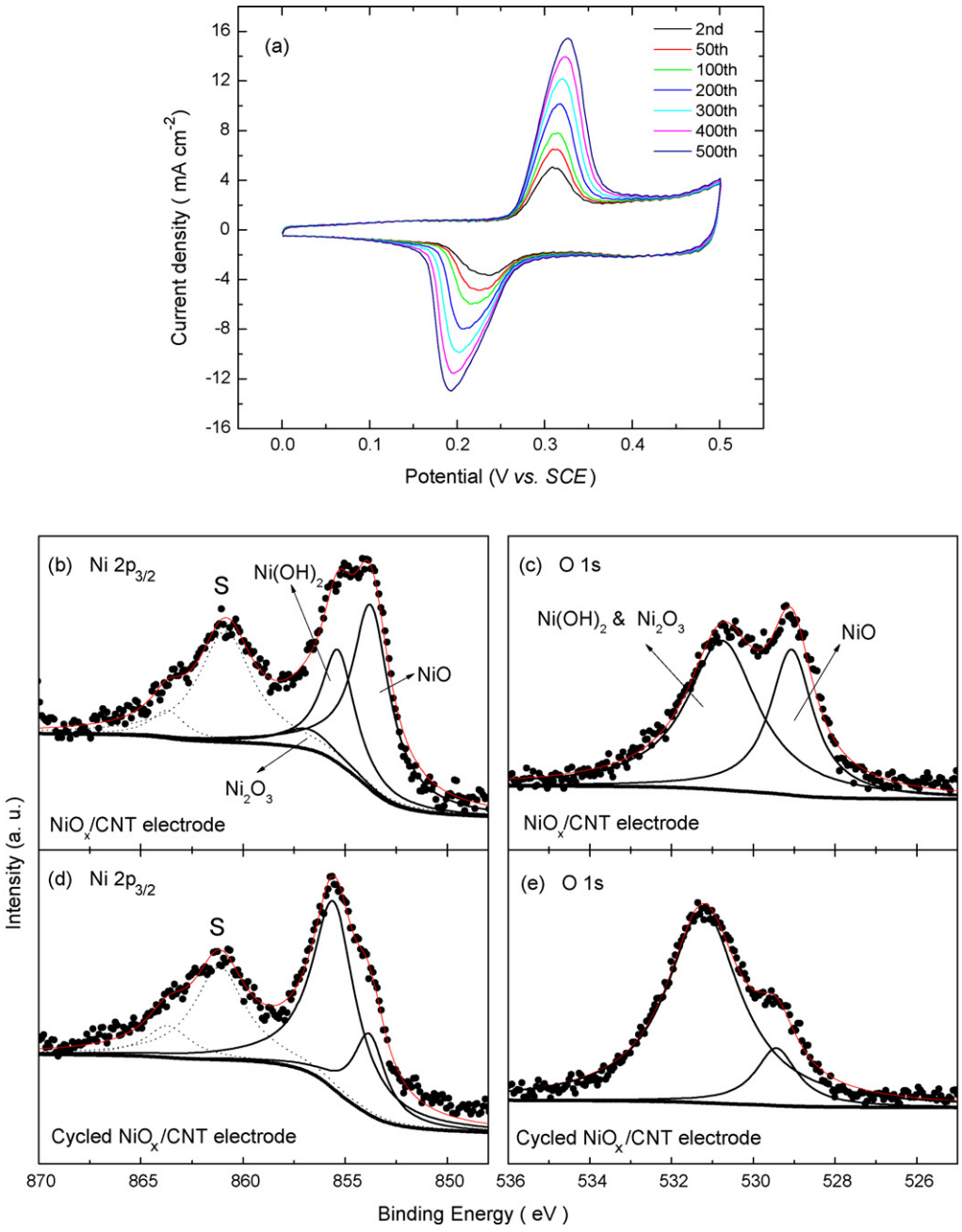

Fig. 4. (a) CVs of the NiO_x/CNT electrode during 500 cycles; X-ray photoelectron spectra of (b) Ni $2p_{3/2}$ and (c) O 1s regions for the as-prepared NiO_x/CNT electrode, and (d) Ni $2p_{3/2}$ and (e) O 1s regions for the cycled NiO_x/CNT electrode. S: satellite peak; solid circle: observed peaks; red line: fitted peaks.

presence of a minor Ni^{3+} component as Ni_2O_3 also supports the non-stoichiometric nature of NiO_x with a cation deficiency. Due to its non-stoichiometry, NiO_x (p-type semiconductor) has a certain level of conductivity depending on the cation vacancy level, which is in contrast to the insulating character of stoichiometric NiO [34]. For example, NiO_x films prepared by RF magnetron sputtering at a substrate temperature of 300 °C in pure oxygen sputtering gas were reported to have a resistivity of 0.22 Ω cm (i.e. a conductivity of 4.54 S cm^{-1}) [34]. After cycling the NiO_x/CNT electrode for 500 CV cycles, the Ni $2p_{3/2}$ XP spectra shown in Fig. 4(d) can be fitted with only two species corresponding to NiO and $Ni(OH)_2$. Furthermore, the relative ratio of $Ni(OH)_2$ increased significantly, which indicates NiO and $Ni(OH)_2$ to be the main components of the cycled NiO_x/CNT electrode. Fig. 4(c) and (e) show the relevant O 1s signals for the as-prepared and cycled NiO_x/CNT electrodes, respectively. The XP spectra show two different peaks at 529.1 and 530.8 eV. The first contribution at ~530 eV was attributed to O^{2-} species from NiO. The component at ~531 eV was assigned to some H_2O surface contamination but also to the possible presence of OH^- species from $Ni(OH)_2$ or Ni_2O_3 [33]. In accordance with the Ni $2p_{3/2}$ XP spectra, there was a higher contribution from $Ni(OH)_2$ after CV cycling with a concomitant decrease in the relative contribution from NiO.

XPS revealed that $Ni(OH)_2$ had formed on the NiO_x/CNT electrode after CV cycling in 1 M KOH. The O/Ni ratios of the as-prepared and cycled NiO_x/CNT electrodes, which were calculated from the Ni $2p_{3/2}$ and O 1S peak areas and sensitivity factors, were 1.06 and 1.45, respectively. The increased O/Ni ratio after CV cycling in 1 M KOH also supports the formation of $Ni(OH)_2$ species. Therefore,

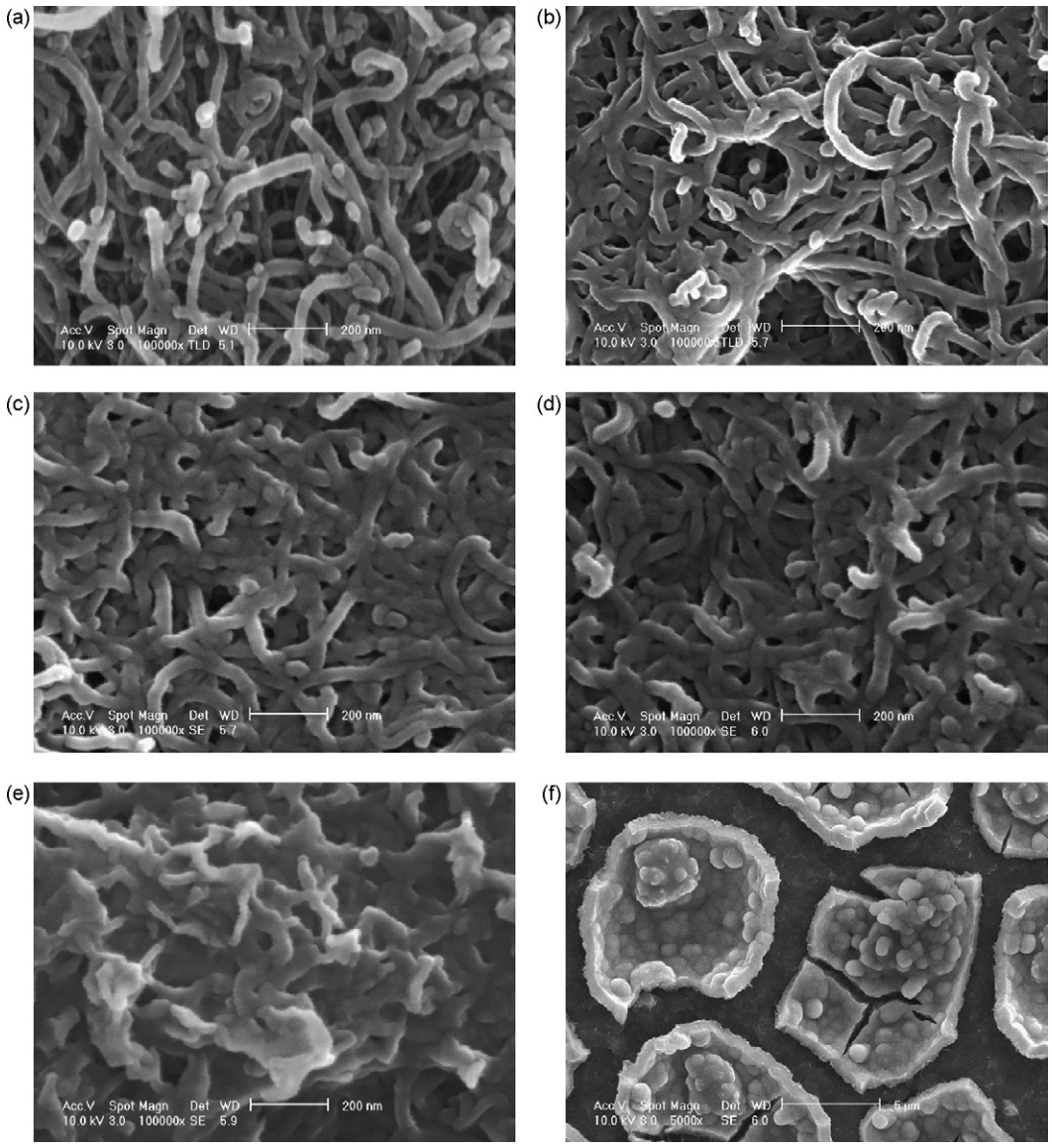

Fig. 5. Top view SEM images of (a) bare CNT film substrate and NiO_x/CNT electrodes with (b) 8.9 wt.%, (c) 11.4 wt.%, (d) 20.2 wt.%, (e) 36.6 wt.%, and (f) 45.8 wt.% of NiO_x. Magnification of all SEM images was 100,000× except for the image (f) for the 45.8 wt.% of NiO_x/CNT electrode, which was taken at 5000×.

the redox peaks appearing in the CVs of the NiO_x/CNT electrodes were attributed to the redox reaction of $Ni(OH)_2$/NiOOH, as shown in reaction (1). This result is also supported by recent reports on electrochromic nickel oxides prepared by pulsed layer deposition, which showed that the most stable Ni(II)-based solid phase should be $Ni(OH)_2$ not NiO [35,36]. Although the $Ni(OH)_2$/NiOOH redox reaction is a bulk redox reaction, it can be applied to supercapacitors if it has rapid reaction kinetics. For example, Nelson et al., reported liquid-crystal-templated mesoporous nickel electrode for supercapacitors using 1–2 nm thick $Ni(OH)_2$ layers on the surface of mesoporous nickel [15]. They claimed that a mesoporous nickel electrode could retain both high energy and power density due to the facile electron and electrolyte transport as well as the extremely small proton diffusion path in the ordered mesoporous structure. Therefore, further studies on the use and control of the $Ni(OH)_2$/NiOOH redox reaction in nanostructured NiO_x electrodes will be needed to improve the energy and power density of nickel based oxide materials for supercapacitors.

3.3. Effect of NiO_x loading amount on the electrochemical properties of the NiO_x/CNT electrodes

The effect of wt.% of NiO_x in the NiO_x/CNT electrode on the microstructure and electrochemical properties was investigated. Fig. 5 shows SEM images of the bare CNT film substrate and NiO_x/CNT electrodes with various wt.% NiO_x. All SEM images were obtained at 100,000× magnification except for that of the NiO_x/CNT electrode containing 45.8 wt.% of NiO_x (Fig. 5(f)), which was taken at 5000× magnification. Fig. 5(a) shows that the bare CNT film substrate consists of individual nanotubes (20–40 nm in diameter) that are entangled to form a uniform web with a 3-dimensional network structure. The SEM images of the NiO_x/CNT electrodes with up to 20.2 wt.% NiO_x showed that a thin NiO_x film had been deposited on the surface of the individual nanotubes, thereby maintaining the 3-dimensional nanoporous structure with its pores unblocked by NiO_x deposits. A previous HR-TEM study on NiO_x/CNT electrodes with a mass fraction of ~20 wt.% showed that the nickel oxides

had nucleated heterogeneously through electrochemical deposition and were deposited on the individual CNTs [23]. Fig. 5(b)–(d) shows a gradual decrease in porosity with increasing wt.% NiO_x. It is expected that the 3-dimensional network structure of NiO_x/CNT electrodes with <20.2 wt.% NiO_x would allow the electrolyte good access throughout the entire thickness of the electrode, a good electrical conduction path through the nanotube network, and an increased oxide/solution interfacial area. On the other hand, pore clogging becomes problematic with further increases in the amount of NiO_x deposited. At 36.6 wt.% and 45.8 wt.% NiO_x, oxide deposits cover the entire CNT film substrate and begin to form on the upper surface of the NiO_x/CNT electrodes. (Fig. 5(e) and (f)) In particular, in the case of the 45.8 wt.% NiO_x/CNT electrode (Fig. 5(f)), the nickel oxides were deposited not only on the individual nanotubes but also on the top outer part of the CNT film surface forming an island structure. The formation of the island structure in the 45.8 wt.% NiO_x/CNT electrode is probably due to shrinkage and cracking of the thick $Ni(OH)_2$ layers deposited on the outer part of the NiO_x/CNT electrode during heating because the phase transformation from $Ni(OH)_2$ to NiO_x during heating at 300 °C is accompanied by ~30% weight loss caused by the removal of absorbed and structural water [12]. On the other hand, the island structure was not observed in the 36.6 wt.% NiO_x/CNT electrode because there was no thick $Ni(OH)_2$ deposits on the outer surface of the 36.6 wt.% NiO_x/CNT electrode. The microstructure of the 36.6 wt.% NiO_x/CNT electrode was examined in more detail by comparing its cross-section SEM image with that of the bare CNT electrode. Fig. 6(a) and (b) shows the cross-section SEM images of the bare CNT and 36.6 wt.% NiO_x/CNT electrodes, respectively. The cross-section SEM image of the bare CNT electrode shows a 3-dimensional network structure with interconnected pores in accordance with the plan view image shown in Fig. 5(a). In contrast, Fig. 6(b) shows that a large part of the 36.6 wt.% NiO_x/CNT electrode consists of agglomerates of NiO_x deposits, which block the interconnected pores, while the small part remaining maintains the 3-dimensional network structure. Although the plan view SEM image of the 36.6 wt.% NiO_x/CNT electrode suggests significant pore clogging, the 3-dimensional network structure is still present to some extent.

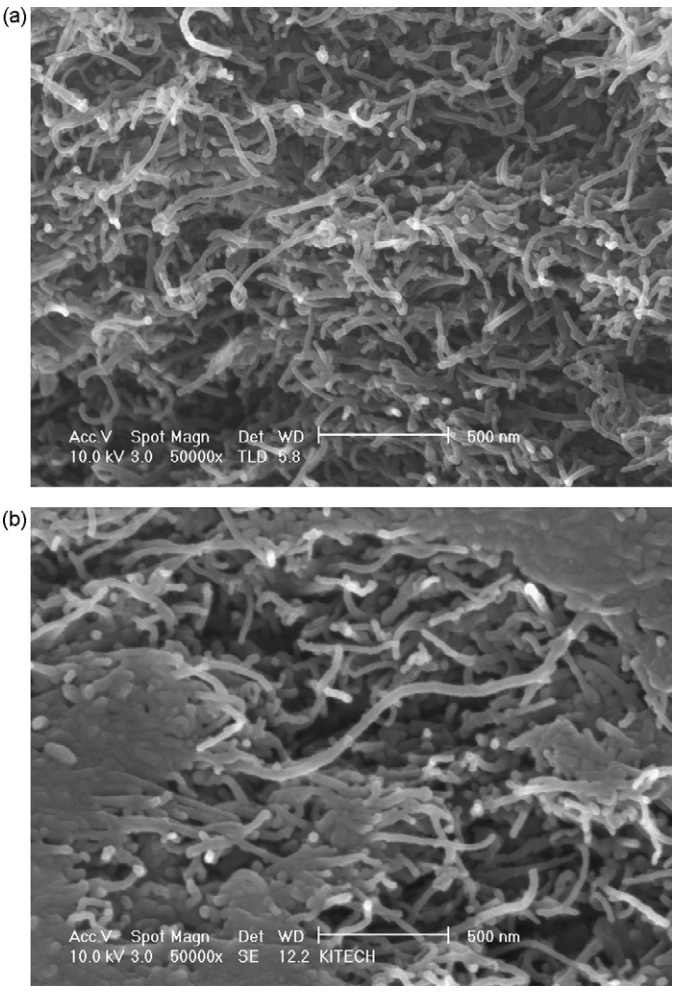

Fig. 6. Cross-sectional SEM images of (a) bare CNT film substrate and (b) 36.6 wt.% NiO_x/CNT electrode. Magnification: 50,000×.

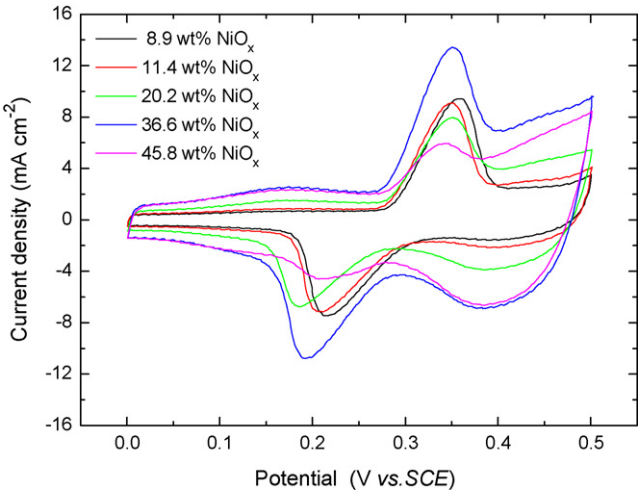

Fig. 7. CVs of the NiO_x/CNT electrodes with various wt.% of NiO_x. The CVs were measured in 1 M KOH at a scan rate of 30 mV s^{-1}.

Cyclic voltammetry was used to determine the electrochemical properties the NiO_x/CNT electrodes as a function of the wt.% of NiO_x. Fig. 7 shows the CVs of the NiO_x/CNT electrodes with different wt.% NiO_x measured at 30 mV s^{-1}. All CVs show capacitive current responses that overlap with the redox peaks corresponding to reaction (1). This suggests that the electrochemically formed $Ni(OH)_2$ does not completely cover the NiO_x surface. It was assumed that $Ni(OH)_2$ forms as nano-particles or nano-domains on the NiO_x surface, thereby exhibiting both electrochemical redox reactions of NiO_x and $Ni(OH)_2$, as indicated in reactions (1) and (2). It was reported that anodic capacitive currents between 0.00 and 0.25 V *vs. SCE* increased with increasing NiO_x concentration up to 36.6 wt.%, and decreased slightly at 45.8 wt.% NiO_x. In contrast, the anodic and cathodic redox peak features were somewhat complicated, and showed a non-monotonic trend with respect to the NiO_x loading.

The complicated electrochemical properties of the NiO_x/CNT electrodes showing current responses from the NiO_x phase as well as the $Ni(OH)_2$ phase were examined by deconvolution analysis of the CVs. As shown in Fig. 8, the total charge of the electrode was deconvoluted into charges from NiO_x (i.e., Q_{NiO_x}) and $Ni(OH)_2$ (i.e., $Q_{Ni(OH)_2}$). Only the cathodic currents were used for deconvolution analysis in order to exclude the contribution of oxygen evolution currents at potentials >~0.45 V *vs. SCE*, which are prominent at low scan rates, such as 10 mV s^{-1}. From the calculated $Q_{Ni(OH)_2}$ value, the mass of $Ni(OH)_2$ formed in the electrode was determined from Faraday's law assuming 100% electrochemical utilization of $Ni(OH)_2$

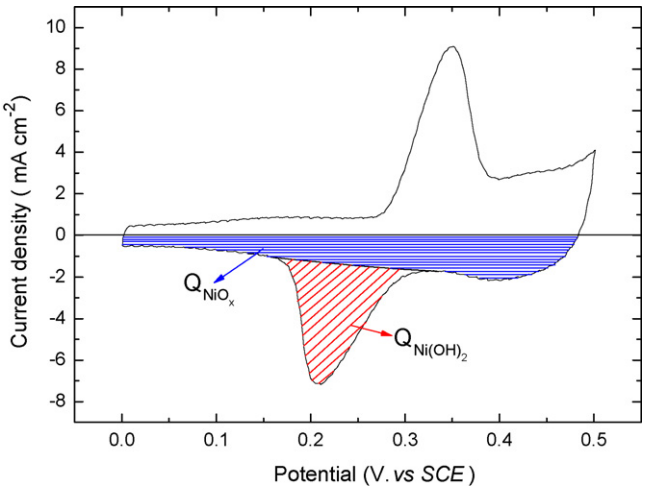

Fig. 8. Schematic diagram of the deconvolution analysis of the CV of the NiO_x/CNT electrode.

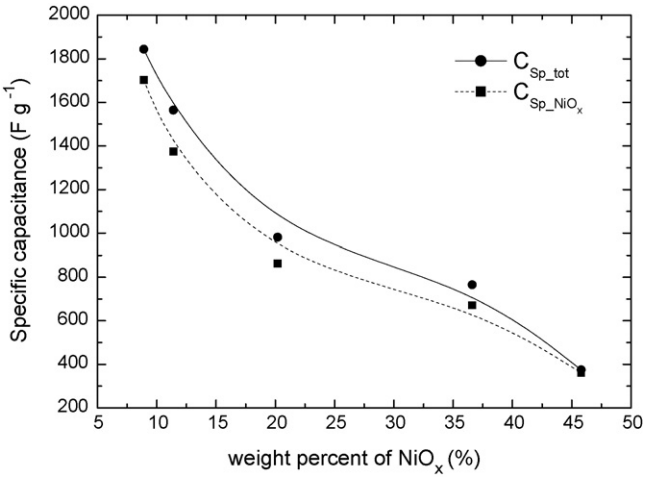

Fig. 10. Total specific capacitance (C_{Sp_tot}) and specific capacitance of NiO_x ($C_{Sp\_NiO_x}$) for the NiO_x/CNT electrodes with various wt.% of NiO_x.

as follows:

$$m = \frac{Q_{Ni(OH)_2} \times M}{F} \quad (3)$$

where m is the mass of $Ni(OH)_2$, $Q_{Ni(OH)_2}$ is the charge obtained from the cathodic peak area in the CVs, M is the molecular weight of $Ni(OH)_2$, and F is Faraday's constant.

Fig. 9 shows the weight ratio of the $Ni(OH)_2$ calculated from Eq. (3), with respect to the weight of NiO_x in the NiO_x/CNT electrodes. Generally, the weight ratios of $Ni(OH)_2$ tends to decrease with increasing wt.% NiO_x. It should be noted that the 8.9 and 11.4 wt.% NiO_x/CNT electrodes contained 42 and 35 wt.% $Ni(OH)_2$, respectively. This indicates a significant contribution from the $Ni(OH)_2$/NiOOH redox reaction to charge storage of the NiO_x/CNT electrodes with a small metal oxide loading. The increase in NiO_x loading up to 36.6 wt.% results in a decrease in the $Ni(OH)_2$ phase concentration in the electrodes. With further increases in the wt.% of NiO_x to 45.8, there was a large decrease in the weight ratio of the $Ni(OH)_2$ phase and only 4 wt.% $Ni(OH)_2$ was observed in the electrode. The SEM images shown in Figs. 5 and 6 indicate that the surface to bulk ratio of the NiO_x/CNT electrodes decreases with increasing wt.% NiO_x. Therefore, the formation of $Ni(OH)_2$ in the nickel oxides is closely related to the high oxide/solution interfacial area. This is supported by the fact that redox peaks were observed in the CVs of the nickel oxides with a high surface/bulk ratio [11,15–17]. The significant decrease in the weight ratio of the $Ni(OH)_2$ phase for the 45.8 wt.% NiO_x/CNT electrode indicates a significant decrease in the oxide/solution interfacial area due to complete pore clogging and deposition on top of the CNT film surface, as observed in the SEM image shown in Fig. 5(f).

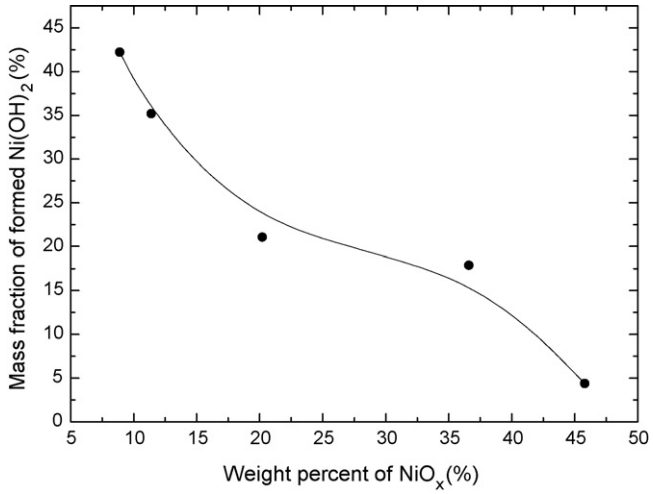

Fig. 9. Weight ratios of the $Ni(OH)_2$ formed with respect to the wt.% of NiO_x in the NiO_x/CNT electrodes.

Fig. 10 shows the specific capacitance of the NiO_x/CNT electrodes, which was calculated from the cathodic charges of the CVs at 30 mV s^{-1}, as a function of the wt.% NiO_x. The total specific capacitance (C_{Sp_tot}) of the NiO_x/CNT electrodes was determined by calculating all the cathodic charges in the CVs, and dividing the result by the potential window of 0.5 V and the mass of the deposited nickel oxide. It should be noted that the mass of the CNT was not considered when calculating the specific capacitance. The specific capacitance contribution from the NiO_x phase $C_{Sp\_NiO_x}$, specific capacitance of NiO_x) was also calculated from Q_{NiO_x} after excluding the charge and mass associated with $Ni(OH)_2$. Fig. 10 shows that both C_{Sp_tot} and $C_{Sp\_NiO_x}$ decrease gradually in a similar manner to the increase in NiO_x wt.%. The NiO_x/CNT electrode with 8.9 wt.% NiO_x showed the highest $C_{Sp\_NiO_x}$ value of 1702 F g^{-1} (for a single electrode). On the other hand, the 45.8 wt.% NiO_x/CNT electrode showed the lowest $C_{Sp\_NiO_x}$ value of 361 F g^{-1}. It should be noted that the $C_{Sp\_NiO_x}$ of 1702 F g^{-1} for the 8.9 wt.% NiO_x/CNT electrode is the highest value reported for nickel oxide electrodes in supercapacitors thus far. The capacitance of the 8.9 wt.% NiO_x/CNT electrode would be reach 1850 F g^{-1} if the total specific capacitance, C_{Sp_tot}, is considered. Since the charge storage reaction of NiO_x is only confined to the oxide surface, a high specific capacitance of NiO_x can be achieved by maximizing the electrochemical utilization by coating an extremely thin NiO_x layer onto a 3-dimensional nanoporous CNT substrate. In contrast, the decrease in the specific capacitance of NiO_x in the NiO_x/CNT electrode with the high NiO_x wt.% is probably due to the increase in the dead volume of the oxides, which increase the ESR for a heavier deposit due to the semiconductivity of NiO_x. The decrease in the specific capacitance of high wt.% NiO_x/CNT electrodes can also be caused by the ineffective supply of ionic species to the oxide surface due to the reduced pore size and pore clogging. This can be expected from the microstructure of the NiO_x/CNT electrodes, as shown in Fig. 5.

A relative comparison of the surface active sites of NiO_x/CNT electrodes could be obtained, even though the real surface area of the NiO_x/CNT electrodes was not measured. The ratio of the measured charge to the total theoretical charge of NiO is related to the

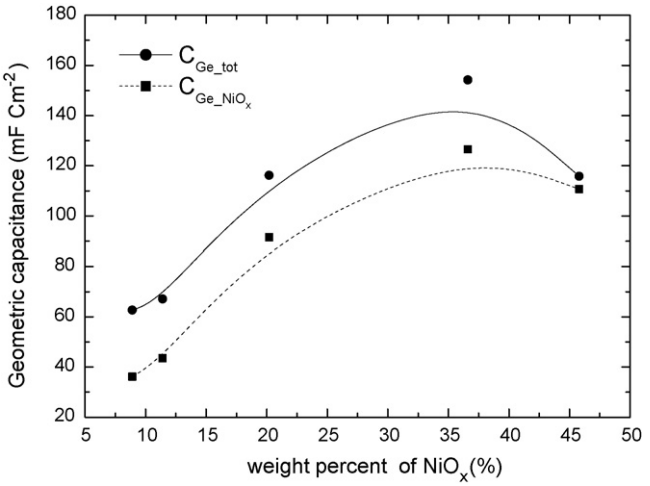

Fig. 11. Total geometric capacitance (C_{Ge_tot}) and geometric capacitance of NiO_x ($C_{Ge\_NiO_x}$)) for the NiO_x/CNT electrodes at various wt.% of NiO_x.

fraction of nickel sites, *z*, involved in the Faradaic reaction, which can be estimated from the specific capacitance of the oxide film using following equation:

$$z = \frac{C_{Sp\_NiO_x} \times \Delta V}{F/M} \quad (4)$$

where ΔV is the potential window (0.5 V in this study), M is the molar weight of NiO (74.7 g mol^{-1}), *F* is the Faraday constant, and $C_{Sp\_NiO_x}$ is the specific capacitance of NiO_x. For example, the *z* value corresponds to 1.0 when all the nickel sites in NiO are involved in the Faradaic reaction of nickel oxide. The calculation using Eq. (4) gave *z* values of 0.66, 0.53, 0.33, 0.26 and 0.14 at 8.9, 11.4, 20.2, 36.6 and 45.8 NiO_x wt.%, respectively. This means that 66, 53, 33, 26 and 14% of the nickel sites participate in the electrochemical reaction of NiO_x electrodes. The highest z value of 0.66 is ~6 times higher than that reported for NiO_x thin films coated on a Pt foil substrate [12,13], which indicates the enhanced electrochemical utilization of the NiO_x/CNT electrode. The 6-fold enhancement in electrochemical utilization was attributed to the unique 3-dimensional network structure of the NiO_x/CNT electrode.

For practical applications, the geometric or volumetric capacitance should also be considered. Since the volume of the CNT film substrates was similar at $\sim 5 \times 10^{-4}$ cm^3 (1 cm × 1 cm × ~5 μm) regardless of the NiO_x wt.%, the volume of the NiO_x/CNT electrodes was $\sim 5 \times 10^{-4}$ cm^3 with the exception of the 46.6 wt.% NiO_x/CNT electrode, where the thick nickel oxides were deposited over the upper surface of the CNT film substrates. Therefore, the volumetric capacitance will be maximized by maximizing the geometric capacitance of the NiO_x/CNT electrodes. Fig. 11 shows the geometric capacitance of the NiO_x/CNT electrodes as a function of the NiO_x loading. The total geometric capacitance (C_{Ge_tot}) and geometric capacitance from the NiO_x phase ($C_{Ge\_NiO_x}$) were calculated by multiplying C_{Sp_tot} and $C_{Sp\_NiO_x}$ by the total mass of the electrode and the mass of NiO_x, respectively. The difference between C_{Ge_tot} and $C_{Ge\_NiO_x}$ is due to the contribution of $Ni(OH)_2$. $C_{Ge\_NiO_x}$ increases gradually with increasing NiO_x loading up to 36.6 wt.%, showing a maximum of 127 mF cm^{-2}, and decreases thereafter. The corresponding volumetric capacitance of the 36.6 wt.% NiO_x/CNT electrode was calculated to be 254 F cc^{-1}, which is ~6 times higher than that of typical activated carbon electrodes used as electrodes for EDLC [37]. If the total geometric capacitance, C_{Ge_tot}, is considered, the volumetric capacitance of the 36.6 wt.% NiO_x/CNT electrode was increased to 320 F cc^{-1}. The high volumetric capacitance of the NiO_x/CNT electrode compared with that of the activated carbon electrodes shows that a nanocomposite of metal oxides and carbon materials is a promising strategy for improving the volumetric capacitance of carbon based electrode materials for electrochemical capacitors. It should be noted that the increase in NiO_x layer thickness on CNTs, which is proportional to the NiO_x wt.% in the electrode, have both a positive and negative effect on the effective surface area (non-normalized by the mass of NiO_x). An increase in the oxide/CNT diameter as a result of the oxide coating will cause an increase in real surface area. On the other hand, a further increase in the oxide coating layer and their contact would result in pore clogging in the CNT web, which will decrease the real surface area. These two effects compete with increasing wt.% NiO_x in the NiO_x/CNT electrodes. In this study, the optimal real surface area was obtained with the 36.6 wt.% NiO_x/CNT electrode, which had the highest geometric and volumetric capacitance.

The rate capability of the NiO_x/CNT electrodes was determined by measuring the normalized capacitance of the various NiO_x wt.% in the electrodes with respect to the scan rate (Fig. 12(a)). The normalized capacitance at each scan rate was obtained by dividing the C_{Sp_tot} of the NiO_x/CNT electrodes at each potential scan rate by the specific capacitance measured at 10 mV s^{-1}. Generally, the normalized capacitance decreases with increasing scan rate. As shown in Fig. 12(a), the decrease in the specific capacitance of the NiO_x/CNT electrodes from 10 to 100 mV s^{-1} at the NiO_x wt.% of 8.9, 11.4, 20.2, 36.6 and 45.8 was 3.8, 6.3, 13.6, 16.9 and 25.6%, respectively. This indicates that the rate capability is inversely proportional to the NiO_x wt.% in the NiO_x/CNT electrodes. This means that a thinner NiO_x layer on the NiO_x/CNT electrodes is more favorable for maintaining a high rate capability. It should be noted that the 8.9 and 11.4 wt.% NiO_x/CNT electrodes showed excellent rate capability, even though they contained >35% $Ni(OH)_2$ for which the electrochemical reaction is diffusion controlled. The SEM images of the 8.9 and 11.4 wt.% NiO_x/CNT electrodes shown in Fig. 5(b) and (c) suggest that the individual CNTs were coated with nickel oxides, a few nm in thickness to form a 3-dimensional network structure. In addition, the $Ni(OH)_2$ phase formed on the electrode is considered to be a nano-particle or nano-domain in an ultrathin semiconductive NiO_x matrix. Therefore, the rapid reaction kinetics of the $Ni(OH)_2$/NiOOH redox reaction is probably due to the unique electrode structure of these NiO_x/CNT electrodes, particularly with a low oxide loading (e.g., 8.9 and 11.4 wt.%). This would result in a lower diffusion path and ESR of the electrode as well as facile ionic transport. In contrast, an increase in the NiO_x coating thickness on the CNT film substrate, which is proportional to the NiO_x loading, would result in an increase in the ESR of the electrode and an insufficient supply of ionic species due to the reduced pore size and pore clogging, thereby causing poor rate capability.

The individual contributions of the redox reactions from NiO_x and $Ni(OH)_2$ on the rate capability were examined by normalizing Q_{NiO_x} and $Q_{Ni(OH)_2}$ with respect to the scan rate at various NiO_x wt.%, as shown in Fig. 12(b) and (c). The normalized charge was obtained by dividing the charges at various scan rates by the charge at 10 mV s^{-1}. It should be noted that the normalized charges of Q_{NiO_x} for the 8.9 and 11.4 wt.% NiO_x/CNT electrodes were >100% at 100 mV s^{-1}. This was attributed to errors in estimating the integration area of the cathodic peak in the CV during deconvolution analysis. It should be noted that the NiO_x redox reaction shows higher rate capability than that of the $Ni(OH)_2$ in the NiO_x/CNT electrode regardless of the wt.% of the NiO_x in the as-prepared NiO_x/CNT electrodes. For example, the normalized charge of NiO_x and $Ni(OH)_2$ in the 20 wt.% NiO_x/CNT electrode decreases by 5 and 40%, respectively when the potential scan rate is changed from 10 to 100 mV s^{-1}. The excellent rate capability of the NiO_x/CNT electrode might be due to the surface redox reaction and p-type conduc-

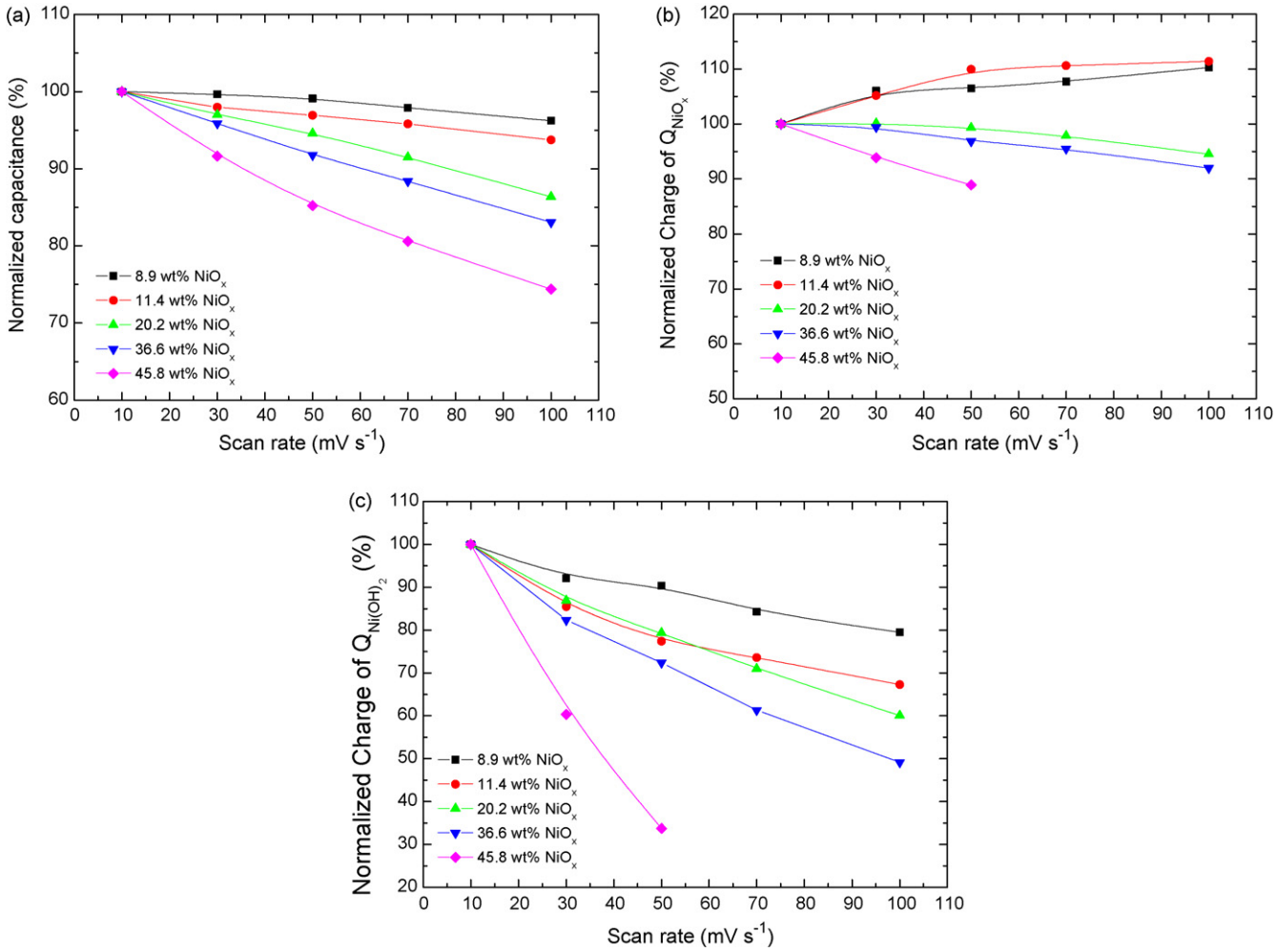

Fig. 12. (a) Normalized total specific capacitance of the NiO_x/CNT electrodes with various wt.% of NiO_x at scan rates from 10 to 100 mV s^{-1}. Normalized charge of (a) NiO_x (Q_{NiO_x}) and $Ni(OH)_2$ ($Q_{Ni(OH)_2}$) phases of the NiO_x/CNT electrodes with various wt.% of NiO_x at scan rates from 10 to 100 mV s^{-1}.

tivity of the NiO_x in addition to the fact that the NiO_x phase is mainly in contact with the electrolyte due to the 3-dimensional solid-pore network structure of the 20 wt.% NiO_x/CNT electrode. On the other hand, the insulating nature and solid-state proton diffusion reaction kinetics of $Ni(OH)_2$ would adversely effect the rate capability of the $Ni(OH)_2$ in the NiO_x/CNT electrode. It is believed that the rate capability of the NiO_x/CNT electrodes is affected more by the $Ni(OH)_2$ redox reaction, which shows a relatively poor rate capability, than that of the NiO_x redox reaction.

A comparison of the rate capability of the $Ni(OH)_2$/CNT electrode in Fig. 3(a) showed that the $Ni(OH)_2$ in the NiO_x/CNT electrode has better rate capability. As shown in Fig. 3(c) and Fig. 12(c), the normalized capacitance of the $Ni(OH)_2$/CNT electrode with 20 wt.% of nickel hydroxide decreases by 90% at 100 mV s^{-1} whereas the normalized charge of $Ni(OH)_2$ in the 20 wt.% NiO_x/CNT electrode decreased by 40% at 100 mV s^{-1}. The superior rate capability of the $Ni(OH)_2$ in the NiO_x/CNT electrode compared with that of the $Ni(OH)_2$/CNT electrode was attributed to the formation of $Ni(OH)_2$ nano-particles or nano-domains surrounded by a semiconducting NiO_x matrix, a few nm in thickness, on the CNTs. It should be noted that the rate capability of the $Ni(OH)_2$ in the NiO_x/CNT electrode is strongly dependent on the wt.% of NiO_x in the NiO_x/CNT electrode, as shown in Fig. 12(c). An increase in the wt.% of NiO_x in the NiO_x/CNT electrode decreased the rate capability of the $Ni(OH)_2$. In the NiO_x/CNT electrode with 45.8 wt.% NiO_x there was a 70% decrease in the normalized charge of $Ni(OH)_2$, even at 50 mV s^{-1}. This is probably due to the formation of a thicker nickel oxide layer over CNTs, which leads to severe pore-clogging in the NiO_x/CNT electrodes with increasing wt.% NiO_x.

4. Conclusions

NiO_x/CNT electrodes with various wt.% of NiO_x were prepared by the electrochemical deposition of $Ni(OH)_2$ onto CNT film substrates followed by heating to 300 °C for 1 h. The detailed electrochemical redox reaction of the NiO_x/CNT electrode in a 1 M KOH solution was examined by XPS and deconvolution analysis of the CVs. A comparison of the electrochemical properties with the as-deposited $Ni(OH)_2$/CNT electrode showed that the NiO_x/CNT electrode with 300 °C heat treatment has high rate capability making it suitable as an electrode material for supercapacitors. XPS showed that the pseudocapacitance of the NiO_x/CNT electrodes originated from both NiO_x/NiO_xOH and $Ni(OH)_2$/NiOOH redox reactions. It was observed that the specific capacitance decreased with increasing wt.% of NiO_x, starting at 8.9% of NiO_x, whereas the geometric and volumetric capacitances increased with increasing wt.% of NiO_x. For example, the 8.9 wt.% NiO_x/CNT electrode showed a NiO_x-normalized specific capacitance of 1701 F g^{-1} with excellent high rate capability. The excellent capacitive behavior of the low

wt.% NiO_x/CNT electrodes was attributed to the construction of a 3-dimensional nanoporous network structure with an extremely thin NiO_x layer on the CNT film substrate. On the other hand, the maximum geometric and volumetric capacitances of 127 mF cm^{-2} and 254 F cc^{-1} were achieved with the 36.6 wt.% NiO_x electrode, which had a lower specific capacitance of 671 F g^{-1}. This decrease in specific capacitance of the high wt.% NiO_x/CNT electrodes is believed to be due to the higher dead volume of oxides, the high ESR for heavier deposits, and ineffective ionic transportation due to the destruction of the 3-dimensional network structure, which is the result of the reduced pore size and pore clogging. Deconvolution analysis of the cyclic voltammograms revealed that the rate capability of the NiO_x/CNT electrodes is adversely affected by the redox reaction of $Ni(OH)_2$, while there are no significant undesirable effects from the reaction of NiO_x. However, in view of the excellent rate capability of NiO_x/CNT electrodes with a low wt.% of NiO_x, which contained a significant amount of $Ni(OH)_2$, it is believed that the deleterious effects on the rate capability caused by $Ni(OH)_2$ can be reduced and the higher specific capacitance of $Ni(OH)_2$ can be utilized if the same three dimensional nanostructure can be achieved. Therefore, the $Ni(OH)_2$/NiOOH redox reaction can be used to improve the energy and power density when nanostructured electrodes are constructed, particularly for NiO_x based electrodes in supercapacitor applications.

Acknowledgements

This work was supported by Korea Science & Engineering Foundation (KOSEF) through the National Research Lab. Program funded by the Ministry of Science and Technology (No. R0A-2007-000-10042-0). The experiments at Brookhaven National Lab. was supported by the Assistant Secretary for Energy Efficiency and Renewable Energy, Office of Vehicle Technologies, under the program of "Hybrid and Electric Systems", of the U.S. Department of Energy under Contract Number DEAC02-98CH10886.

References

[1] B.E. Conway, Electrochemical Supercapacitors; Scientific Fundamentals and Technological Applications, Kluwer Academic/Plenum Publishers, New York, 1999.
[2] E. Frackowiak, Phys. Chem. Chem. Phys. 9 (2007) 1774–1785.
[3] J.P. Zheng, P.J. Cygan, T.R. Zow, J. Electrochem. Soc. 142 (1995) L6–L8.
[4] C. Lin, J.A. Ritter, B.N. Popov, J. Electrochem. Soc. 145 (1998) 4097–4103.
[5] M. Toupin, T. Brousse, D. Belanger, Chem. Mater. 14 (2002) 3946–3952.
[6] C.C. Hu, T.W. Tsou, Electrochem. Comm. 4 (2002) 105–109.
[7] V. Subramanian, H.W. Zhu, R. Vajtai, P.M. Ajayan, B.Q. Wei, J. Phys. Chem. B 109 (2005) 20207–20214.
[8] S.B. Ma, Y.H. Lee, K.Y. Ahn, C.M. Kim, K.H. Oh, K.B. Kim, J. Electrochem. Soc. 153 (2006) C27–C32.
[9] K.W. Nam, M.G. Kim, K.B. Kim, J. Phys. Chem. C 111 (2007) 749–758.
[10] K.C. Liu, M.A. Anderson, J. Electrochem. Soc. 143 (1996) 124–130.
[11] V. Srinivasan, J.W. Weidner, J. Electrochem. Soc. 144 (1997) L210–L213.
[12] K.W. Nam, K.B. Kim, J. Electrochem. Soc. (2002) A346–A354.
[13] K.W. Nam, W.S. Yoon, K.B. Kim, Electrochim. Acta 47 (2002) 3201–3209.
[14] J. Cheng, G.P. Gao, Y.S. Yang, J. Power Sources 159 (2006) 734–741.
[15] P.A. Nelson, J.R. Owen, J. Electrochem. Soc. 150 (2003) A1313–A1317.
[16] F.B. Zhang, Y.K. Zhou, H.L. Li, Mater. Chem. Phys. 83 (2004) 260–264.
[17] Y.G. Wang, Y.Y. Xia, Electrochim. Acta 51 (2006) 3223–3227.
[18] G.G. Amatucci, F. Badway, A.D. Pasquier, T. Zheng, J. Electrochem. Soc. 148 (2001) A930–A939.
[19] J.H. Park, O.O. Park, K.H. Shin, C.S. Jin, J.H. Kim, Electrochem. Solid State Lett. 5 (2002) H7–H10.
[20] V. Ganesh, S. Pitchumani, V. Lakshminarayanan, J. Power Sources 158 (2006) 1523–1532.
[21] C.C. Hu, W.C. Chen, K.H. Chang, J. Electrochem. Soc. 151 (2004) A281–A290.
[22] J.H. Park, J.M. Ko, O.O. Park, J. Electrochem. Soc. 150 (2003) A864–A867.
[23] K.W. Nam, E.S. Lee, J.H. Kim, Y.H. Lee, K.B. Kim, J. Electrochem. Soc. 152 (2005) A2129–A2139.
[24] A.E. Fischer, K.A. Pettigrew, D.R. Rolison, R.M. Stroud, J.W. Long, Nano Lett. 7 (2007) 281–286.
[25] Y.T. Wu, C.C. Hu, J. Electrochem. Soc. 151 (2004) A2060–A2066.
[26] J.S. Sakamoto, B. Dunn, J. Electrochem. Soc. 149 (2002) A26–A30.
[27] I.H. Kim, J.H. Kim, B.W. Cho, K.B. Kim, J. Electrochem. Soc. 153 (2006) A989–A996.
[28] I.H. Kim, J.H. Kim, B.W. Cho, K.B. Kim, J. Electrochem. Soc. 153 (2006) A1451–A1458.
[29] J.H. Kim, K.W. Nam, S.B. Ma, K.B. Kim, Carbon 44 (2006) 1963–1968.
[30] A. Cao, C. Xu, J. Liang, D. Wu, B. Wei, Chem. Phys. Lett. 344 (2001) 13–17.
[31] A. Motori, F. Sandrolini, G. Davolio, J. Power Sources 48 (1994) 361–370.
[32] J.G. Kim, D.L. Pugmire, D. Battaglia, M.A. Langell, Appl. Surf. Sci. 165 (2000) 70–84.
[33] B.A. Reguig, M. Reragui, M. Morsli, A. Khelil, M. Addou, J.C. Bernede, Sol. Energy Mater. Sol. Cells 90 (2006) 1381–1392.
[34] Y.M. Lu, W.S. Hwang, J.S. Yang, Surf. Coat. Technol. 155 (2002) 231–235.
[35] I. Bouessay, A. Rougier, J.-M. Tarascon, J. Electrochem. Soc. 151 (2004) H145–H152.
[36] I. Bouessay, A. Rougier, P. Poizot, J. Moscovici, A. Michalowicz, J.-M. Tarascon, Electrochim. Acta 50 (2005) 3737–3745.
[37] C. Emmenegger, P. Mauron, P. Sudan, P. Wenger, V. Hermann, R. Gallay, A. Züttel, J. Power Sources 124 (2003) 321–329.